WRF–City–LES Modelling of the Urban Thermal Environment in Sofia

Ryota Karube[1, 2], Lidia Lazarova Vitanova [1]*, Evgeny Shirinyan[1], Takuto Sato[3], Dessislava Petrova-Antonova[1], Hiroyuki Kusaka[3]

[1] GATE Institute, Sofia University "St. Kliment Ohridski", Sofia, Bulgaria
{ryota.karube, lidia.vitanova, evgeny.shirinyan, dessislava.petrova}@gate-ai.eu

[2] Graduate School of Science and Technology, University of Tsukuba, Ibaraki, Japan
{s2530306}@u.tsukuba.ac.jp

[3] Center for Computational Sciences, University of Tsukuba, Ibaraki, Japan
{sato.takuto.gu}@u.tsukuba.ac.jp {kusaka}@ccs.tsukuba.ac.jp

Keywords: Weather Research and Forecasting (WRF) model, City-LES model, Temperature, Urban Heat Island

Abstract

Urban areas are increasingly exposed to thermal stress owing to the combined effects of global warming and the Urban Heat Island (UHI). High-resolution numerical modelling is therefore needed to assess local thermal environments and support heat-mitigation planning. This study applies a high-resolution WRF–City-LES downscaling approach to simulate the urban thermal environment of Sofia, Bulgaria. The mesoscale Weather Research and Forecasting (WRF) model provides regional- to urban-scale meteorological forcing, whereas the microscale City-LES model resolves city-block-scale thermal and wind environments in the Lozenets district by explicitly representing buildings, trees, land-surface characteristics, and building-related anthropogenic heat (AH). Compared with the mesoscale WRF simulation, City-LES more accurately represents the near-surface air temperature at the observation sites, reducing the mean absolute error (MAE) from 1.4 °C to 0.3 °C and the root mean square error (RMSE) from 1.4 °C to 0.3 °C. The high-resolution micro-simulation also captures fine-scale spatial variability in near-surface air temperature and outdoor thermal comfort that WRF did not resolve. The spatial distributions of Mean Radiant Temperature (MRT) and Universal Thermal Climate Index (UTCI) reveal city-block-scale differences related to buildings, tree canopies, and radiative conditions. The AH sensitivity experiment showed that building-related AH had a limited effect on domain-averaged near-surface air temperature under the present implementation. These results demonstrate that the WRF–City-LES downscaling approach provides a useful basis for urban climate assessment and future urban digital twin applications, including scenario-based evaluation of heat-mitigation strategies.

1. Introduction

Urban areas are increasingly exposed to thermal stress owing to the combined effects of global warming and the Urban Heat Island (UHI) phenomenon, posing serious risks to public health and quality of life (Assenova et al., 2024). Numerical modelling offers a flexible means of evaluating urban thermal environments and assessing heat-mitigation strategies under diverse scenarios, advantages that observational studies inherently cannot provide (Vitanova et al., 2026).

Mesoscale meteorological models, which typically represent urban-scale atmospheric conditions at horizontal resolutions of approximately 1–10 km, are useful for assessing urban-scale thermal environments under realistic regional meteorological conditions (Nishi et al., 2019). However, their spatial resolution is generally insufficient to resolve microscale, city-block-scale thermal environments at approximately 1–10 m resolution, where temperature, wind, and radiation fields are strongly affected by buildings, street geometry, vegetation, surface materials, and Anthropogenic Heat (AH) emissions.

To bridge the gap between urban-scale meteorological conditions and city-block-scale thermal environments, downscaling approaches are required (e.g., Vogel et al., 2022). Downscaling can broadly be classified into statistical and dynamical approaches. Statistical downscaling estimates local-scale climate variables from larger-scale meteorological conditions using empirical relationships between coarse-resolution model-grid values and observations at selected sites (e.g., Wilby and Wigley, 1997). Although this approach can be effective when dense and long-term observations are available, its application to city-block-scale urban thermal environments is limited. This is because such environments are highly spatially heterogeneous, and resolving the effects of complex urban morphology would require many observation sites within city blocks. In addition, spatial interpolation is generally insufficient to represent sharp variations in temperature, wind, and radiation caused by buildings, street geometry, and vegetation.

Dynamical downscaling, in contrast, employs physically based numerical models to generate higher-resolution meteorological fields from larger-scale atmospheric conditions (Giorgi and Mearns, 1991). This approach, using microscale urban meteorological models, is particularly suitable for simulating city-block-scale meteorological conditions because buildings, vegetation, and turbulent transport can be explicitly represented in the microscale model. Recently, Large-Eddy Simulation (LES) has emerged as a superior approach for resolving turbulent large eddies that are essential for heat and momentum transport at the microscale. The "PALM model system" (Maronga et al., 2020) and "City-LES" (Ikeda et al., 2015; Kusaka et al., 2024) are LES model for urban areas and explicitly resolve buildings and vegetation. In the present study, "City-LES" is adopted as the microscale urban meteorological model for dynamical downscaling, while mesoscale meteorological fields are simulated by the Weather Research and Forecasting (WRF) model to create meteorological forcing for City-LES.

Recent applications of mesoscale–microscale dynamical downscaling include WRF–PALM-4U simulations in Berlin, Germany (Vogel et al., 2022), and WRF-Chem–PALM-4simulations in the KAUST region, Saudi Arabia (Thiruridathil et al., 2024). Although such frameworks have demonstrated the

* Corresponding author

https://doi.org/10.5194/isprs-archives-L-4-W3-2026-67-2026

feasibility of mesoscale-to-microscale coupling, their validation and applicability across diverse urban morphologies and climatic regions remain active research issues (e.g., Liu et al., 2025). Furthermore, relying on a single modelling approach may overlook inherent biases in the model. Using multiple modelling frameworks is increasingly necessary to cross-validate findings and capture urban climate processes that a single model might miss, enabling future multi-model ensemble simulations.
Against this background, the present study represents the first application of a high-resolution WRF–City-LES dynamical downscaling approach to simulating the urban thermal environment of Sofia, Bulgaria. The study covers the Lozenets district, which features dense building structures, green spaces, and complex urban morphology. Sofia has experienced substantial urban growth in recent decades (Vitanova et al., 2026), intensifying UHI effects and heat-related health risks (Vitanova et al., 2021). Previous WRF-based studies reported nighttime temperature increases of up to 3.4 °C in the city centre due to land-use change, and a surface air temperature rise of approximately 4.0 °C since 1878, when combined with AH (Vitanova and Kusaka, 2018; Vitanova et al., 2021).

The study addresses the following research questions (RQ):

RQ1: To what extent can a high-resolution downscale modelling approach based on City-LES improve the understanding of the urban thermal environment in Sofia?

RQ2: How do urban morphology, land surface characteristics, and AH influence local temperature patterns of Sofia?

RQ3: What local variations and fine-scale urban climate processes, remaining unresolved by conventional mesoscale models, can be revealed through high-resolution microscale simulations?

The results of the study can support urban planning and decision-making by identifying heat-vulnerable areas and assessing how urban form and land use influence local temperatures. Furthermore, such high-resolution downscaling approach based on WRF and City-LES provides a foundation for further development of Urban Digital Twin (UDT) applications. It enables what-if scenario analysis and the evaluation of heat-mitigation strategies.

The paper is organised as follows. Section 2 describes the data and the methodology used to implement the study, including an introduction to the study area, data collection and preparation, and the configuration of the WRF–City-LES. Section 3 presents the results obtained, discussing model validation, thermal comfort evaluation, and the effect of AH. Section 4 concludes the paper, providing directions for future work.

2. Data and Methodology

This section outlines the study area, data collection and preprocessing, model configuration, and validation of simulation results against observational data. Figure 1 shows the overall study workflow.

2.1 Study Area

The study focuses on Sofia city, the capital of Bulgaria. Figure 2 shows the city boundary and traffic network used to describe the urban context. The traffic network was obtained from TomTom (TomTom, 2024), and the city boundary was provided by Sofia Municipality (Sofia Municipality, 2009).

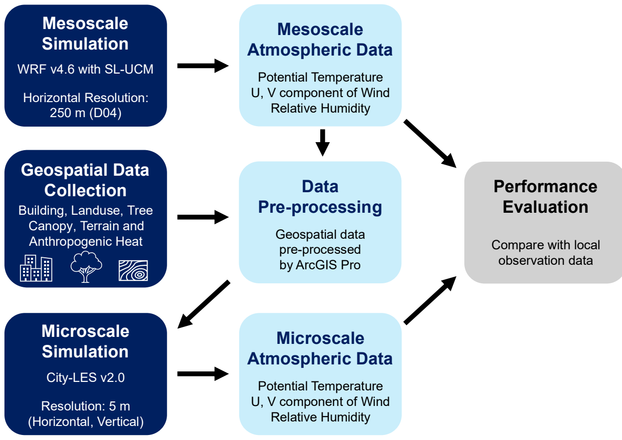

Figure 1. Study workflow for the high-resolution downscaling approach based on WRF and City-LES.

Geographically, Sofia is situated within the Sofia Valley, a well-defined basin that accommodates intensive urban development while maintaining agricultural land uses in its peripheral and surrounding areas. Over the past two decades, the city has experienced steady population growth, with its population approaching 1.3 million by 2024, accounting for approximately 20% of the country's total population (World Population Review, 2024).

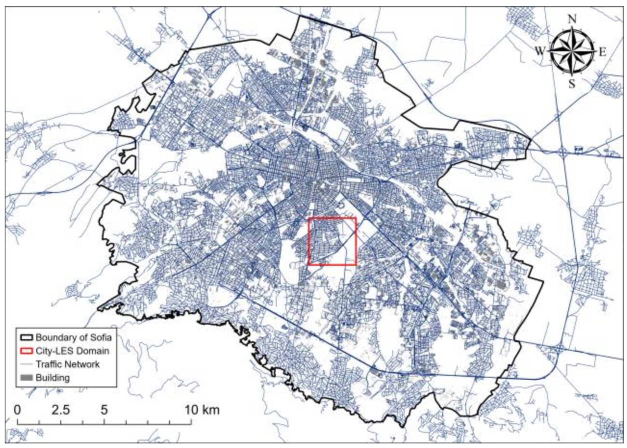

Figure 2. Study area.

2.2 Data Collection and Preparation

This section presents the geospatial datasets used to prepare the input data for the City-LES simulation, including building geometry, land cover classification, terrain elevation, tree canopy information, and AH emissions.

Buildings: The building footprints was gathered from the open data portal of the Cadastral agency (Geoportal of Geodesy, Cartography and Cadastre Agency, 2024). Building heights were acquired from a photogrammetric point cloud. Building parts within a footprint were extracted from a raster Digital Surface Model with a Segment Mean Shift algorithm in ArcGIS Pro. Further, the segmented building footprints were extruded in Rhino using the Heron plugin and aggregated into watertight solid bodies using a grouping field with a unique building identifier (Washburn, 2020). The resulting geometry was converted to ESRI Multipatch format.

Land cover: To classify land cover types, an orthophoto (0.1 m/pixel) was used from an aerial survey conducted in the autumn of 2020. The dataset was clipped to the domain boundary. Six categories of various land cover types were then outlined and fed into an image classification process using the Support Vector Machine algorithm within ArcGIS Pro. High vegetation was excluded from consideration. The street polygons were provided in vector format. After the preliminary classification, land cover data were polygonised to refine the areas, with vector polygons explicitly representing building footprints and street surfaces.

Terrain: The terrain surface was represented using a Digital Terrain Model (DTM). The DTM was provided as a raster dataset with a spatial resolution of 1 m/pixel and was clipped to the model domain boundary.

Tree Canopy: Tree canopy data were obtained from the Tree Map of Sofia, a municipal tree dataset that provides basic but reliable information on trees within Sofia, with an estimated accuracy of approximately 80%. The orthophoto was utilised for detection of tree locations. Tree crown boundaries in 95% of the images and the type of tree (deciduous or conifer) were identified. Tree heights were derived from a photogrammetric point cloud of the Lozenets district.

Anthropogenic Heat: AH emissions were approximated using building energy consumption data obtained from energy performance certificates (EPCs) (Agency for Sustainable Energy Development, 2025). To extrapolate data from EPCs, a method described in Vitanova et al. (2023) and Koleva et al. (2024) was applied and manually refined for specific buildings in the area. For simplicity, building energy consumption was treated as heat released from buildings into the outdoor urban environment. The emissions were spatially allocated within the model domain based on building footprints, and their temporal variation was prescribed as in Vitanova and Kusaka (2018). The resulting AH emissions were incorporated as input data in the City-LES simulation.

The collected geospatial datasets were pre-processed in ArcGIS Pro to generate grid-based input attributes for the City-LES model. The City-LES model grid was represented as point data, and spatial attributes, including building geometry, land-use classification, tree canopy information, and AH emissions, were assigned to each grid point using spatial joins. These procedures ensured spatial consistency among the heterogeneous geospatial datasets and the City-LES computational grid.

Terrain elevation was not directly used as input data for the City-LES simulation. Instead, it was used only during post-processing to correct simulated air temperature and relative humidity for elevation differences between the model grid points and the corresponding observation points.

2.3 Configuration of the WRF–City-LES

The configurations and roles of the mesoscale WRF model and the microscale City-LES model in the downscaling framework are summarized in Table 1.

WRF was used to simulate regional- to urban-scale meteorological fields under realistic regional meteorological conditions, whereas City-LES was used to simulate city-block-scale thermal and wind environments within the target urban district. Thus, WRF provides the urban-scale meteorological context, while City-LES resolves city-block-scale urban processes that the mesoscale model cannot explicitly represent.

For the City-LES, output from the innermost WRF domain with a horizontal spacing of 250 × 250 was used. WRF downward shortwave and longwave radiation from 06:00 to 20:00 EEST on 16 July 2024 were prescribed as time-varying radiative forcing, whereas WRF atmospheric fields at 19:00 EEST were used as the initial and fixed lateral boundary conditions for the 1 h dynamic simulation. In WRF, AH flux was prescribed to exhibit diurnal variation based on Sofia's electricity consumption, following Vitanova and Kusaka (2018), and was introduced into the first atmospheric layer following Khanh et al. (2023).

The City-LES model version 2.0 (Kusaka et al., 2024) was used to perform microscale simulation of the Lozenets district. The City-LES domain covered a 2000 m × 2000 m × 3000 m area centered at 42.6739° N and 23.3306° E. City-LES explicitly represents urban canopy elements, such as buildings and trees, and simulates three-dimensional airflow, surface energy processes, and radiative transfer within the urban canopy. The subgrid-scale eddies were parameterized using the Smagorinsky model (Smagorinsky, 1963).

WRF-derived downward shortwave and longwave radiation were used as forcing for the City-LES, while three-dimensional radiation within the urban canopy layer was calculated using the radiosity method in the City-LES (Sparrow and Cess, 1978). Surface temperature was calculated using a surface heat budget model, and turbulent heat fluxes were estimated using a bulk transfer method (Mascart, 1995).

The simulation date and time window were selected based on the occurrence of a hot summer day and the WRF-simulated UHI pattern. The date, 16 July 2024, was one of the hottest days of the year, and the 19:00–20:00 EEST time window was selected because the WRF simulation indicated a pronounced UHI pattern during this period, characterized by a clear temperature contrast between vegetated areas and built-up urban blocks. This period was therefore considered suitable for evaluating whether City-LES could resolve fine-scale thermal variation associated with urban morphology and land-surface characteristics.

The City-LES simulation consisted of a 13 h surface spin-up simulation and a subsequent 1 h dynamic simulation. During the surface spin-up, which was initialized at 06:00 EEST on 16 July 2024, atmospheric dynamic processes were not computed. Instead, near-surface meteorological variables from WRF, including air temperature, humidity, wind speed, downward shortwave radiation, and downward longwave radiation, were prescribed as external forcing to adjust the thermal conditions of the land surface and urban canopy. After the surface spin-up, the dynamic simulation was initialized at 19:00 EEST on 16 July 2024 using WRF output and integrated for 1 h. Fixed lateral boundary conditions based on the WRF output were applied to the City-LES domain.

Since the WRF boundary fields do not explicitly include LES-scale turbulent fluctuations, artificial inflow turbulence was generated using the cell perturbation method of Muñoz-Esparza et al. (2014), with the parameter settings following Lee et al. (2019) and Sato and Kusaka (2023).

The geospatial input parameters used in the City-LES simulation, including building height, tree canopy, land-use classification, and AH, are shown in Figure 3, together with the terrain elevation data used for post-processing. Although City-LES can represent terrain using a step-like surface, the present simulation was conducted over flat terrain.

Terrain elevation was therefore not used as direct input to City-LES but was used only for post-processing corrections of simulated air temperature and relative humidity, as described in Section 2.2.

https://doi.org/10.5194/isprs-archives-L-4-W3-2026-67-2026 | © Author(s) 2026. CC BY 4.0 License.

	Mesoscale model	Microscale model
Model	WRF-ARW version 4.6 (Skamarock et al., 2019)	City-LES version 2.0 (Kusaka et al., 2024)
Main role	Simulating regional- to urban-scale meteorological fields	Simulating city-block-scale thermal and wind environments
Target scale	Mesoscale / urban scale	Microscale / city-block scale
Horizontal grid spacing	D01: 6.75 km, D02: 2.25 km D03: 0.75 km, D04: 0.25 km	5 m
Number of vertical layers	35 layers	600 layers
Domain size (x, y)	D01: 100 × 100, D02: 124 × 124 D03: 238 × 238, D04: 238 × 238	400 × 400
Simulation period	14 July 2024 18:00 UTC to 22 July 2024 00:00 UTC	Surface spin-up: 06:00–19:00 EEST, 16 July 2024 dynamics: 19:00–20:00 EEST, 16 July 2024
Initial and boundary conditions	NCEP-FNL Operational Global Analysis (National Centers for Environmental Prediction, 2000)	WRF simulation result with artificial turbulence estimated by Cell perturbation method (Muñoz-Esparza et al., 2014)
Urban representation	Single-layer urban canopy model (Kusaka et al., 2001; Kusaka and Kimura, 2004; Chen et al., 2011)	Explicit representation of buildings and trees
Land surface / surface energy process	Noah-LSM (Chen et al., 2011)	Surface heat budget model
Radiation	Shortwave: Dudhia scheme (Dudhia, 1989) Longwave: RRTM scheme (Mlawer et al., 1997)	WRF-derived downward radiation used as forcing; 3D radiation in urban-canopy layer was calculated with radiosity method (Sparrow and Cess, 1978)
Turbulence	Mellor–Yamada–Janjic TKE scheme (Janjić, 1994)	LES with subgrid-scale eddies parameterized using the Smagorinsky model (Smagorinsky, 1963)
Microphysics	WSM 6-class graupel scheme (Hong et al., 2004)	—
Cumulus parameterization	Kain–Fritsch scheme in D01 only (Kain, 2004)	—

Table 1. Configuration and roles of the mesoscale WRF and microscale City-LES models in the downscaling pipelines.

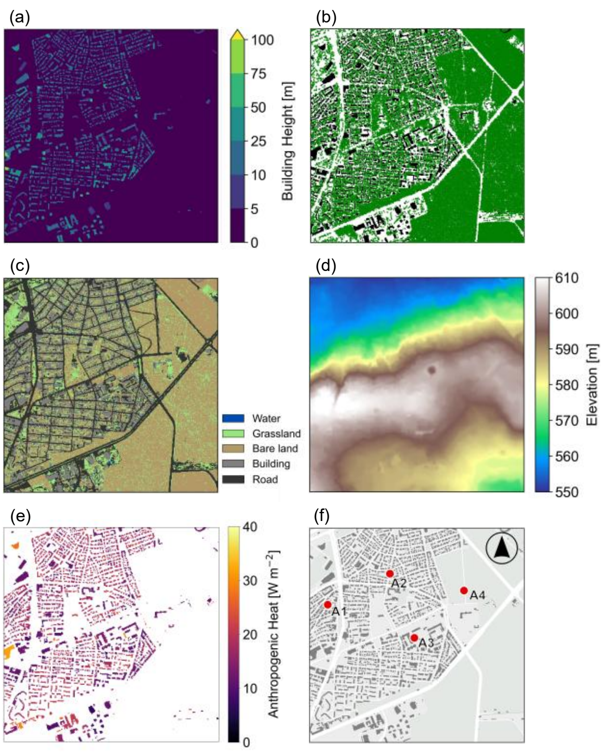

Figure 3. Study area for the City-LES model. (a) Building height [m], (b) tree canopy, (c) land-use classification, (d) terrain elevation, (e) anthropogenic heat, and (f) observation sites.Model validation of the WRF and City-LES models

The WRF and City-LES simulation results were evaluated using local meteorological observations obtained from the City Living Lab sensor network operated by the GATE Institute (City Living Lab, 2024). The sensors were installed at selected monitoring sites in the Lozenets district, and their locations are shown in Figure 3(f). The observational dataset included near-surface air temperature, relative humidity, and wind speed. For validation, simulated values were extracted at the model grid points nearest to each observation site and compared with the corresponding observations. Air temperature and relative humidity were corrected for elevation differences between the model grid points and observation sites, as described in Section 2.2.

3. Results and Discussion

This section presents the results of the WRF–City-LES downscaling simulation for the Lozenets district and discusses how the simulated urban thermal environment varies within the district. The discussion focuses on differences between City-LES and WRF, local variations associated with land cover, buildings, and tree canopies, and the sensitivity of near-surface air temperature to building-related AH.

3.1 Model Validation

The horizontal distributions of near-surface air temperature simulated by City-LES and WRF are shown in Figure 4. The high-resolution City-LES simulation resolved fine-scale spatial variations within the urban district (Figure 4a). In the City-LES result, the temperature ranged from 27.7 to 34.0 °C, with a spatial standard deviation of 1.0 °C. In contrast, the mesoscale WRF simulation produced a smoother temperature field (Figure 4b). The temperature, obtained by the WRF model, ranged from 31.2 to 33.0 °C, with a spatial standard deviation of 0.6 °C. The comparison of the temperature range and spatial standard deviation shows that City-LES represented a wider range of local temperature variations than WRF within the target district.

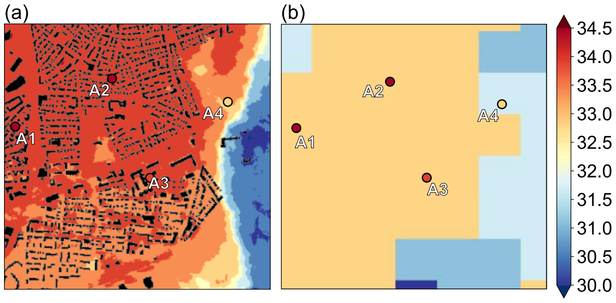

Figure 4. Horizontal distribution of near-surface air temperature [°C] in the Lozenets district, Sofia, on 16 July 2024: (a) high-resolution City-LES result averaged from 19:50 to 20:00 EEST and (b) mesoscale WRF result at 20:00 EEST.

The greater spatial variability in the City-LES results is likely due to differences in spatial resolution and urban representation between the two models. City-LES explicitly represents individual buildings, street geometry, and tree canopies, whereas WRF represents urban effects through a bulk urban canopy model at a coarser horizontal grid spacing. In the City-LES result, relatively higher near-surface air temperatures were found over roads and near buildings, while lower temperatures were observed over grassland and other vegetated areas. The domain-averaged temperature was 33.0 °C over grassland, 33.4 °C over roads, and 33.6 °C in building-adjacent areas. The differences among these land-cover and urban-surface categories suggest that land cover and building-scale urban morphology can influence near-surface air temperature at the city-block scale.

The simulated near-surface air temperatures were evaluated against local observations at the four observation sites (City Living Lab, 2024) (Figure 5). The MAE, RMSE, and Pearson correlation coefficient (r) were used as quantitative evaluation metrics. Compared with the mesoscale WRF simulation, the high-resolution WRF–City-LES simulation substantially reduced the MAE from 1.4 °C to 0.3 °C and the RMSE from 1.4 °C to 0.3 °C, while maintaining a high correlation with the observations (r = 0.997). The comparison with observations indicates that City-LES improved the representation of near-surface air temperature at the observation sites.

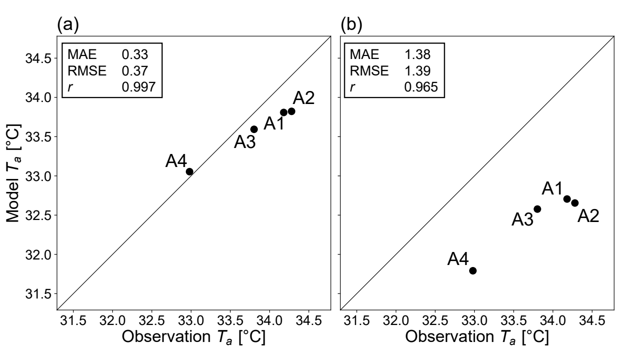

Figure 5. Scatter plots comparing observed and simulated near-surface air temperature [°C] at four stations (A1–A4). An average of 10 min from 19:50–20:00 LST on 16 July 2024. The MAE, RMSE, and correlation coefficient for (a) City-LES and (b) WRF are shown.

The available observations were limited to four sites and did not cover the relatively cooler southern part of the clipped domain. Therefore, the present validation mainly supports the model performance at the observation sites. Additional observations would be useful for assessing the full spatial variability simulated by City-LES.

3.2 Evaluation of Thermal Comfort

Outdoor thermal comfort was evaluated using the Mean Radiant Temperature (MRT) and the Universal Thermal Climate Index (UTCI). MRT was used to assess spatial variability in radiative exposure, whereas UTCI was used as an integrated heat-stress index based on air temperature, humidity, wind speed, and radiation (Bröde et al., 2012). For the WRF output, MRT was calculated from the simulated meteorological and radiative variables following Kacker et al. (2024), as also adopted by Wei and Sobrino (2025), and UTCI was then derived using the same formulation applied to the City-LES output.

The spatial distributions of MRT and UTCI simulated by City-LES and WRF are shown in Figures 6 and 7. For MRT, the City-LES result showed clear spatial variability within the clipped domain, with values ranging from 25.1 °C to 36.5 °C and a spatial standard deviation of 1.8 °C (Figure 6a). In contrast, the WRF-derived MRT field was more uniform, ranging from 38.4 °C to 40.0 °C at the grid points intersecting the clipped domain (Figure 6b). For UTCI, City-LES also showed clear spatial variability, with values ranging from 29.1 °C to 32.4 °C and a spatial standard deviation of 0.5 °C (Figure 7a). The WRF-derived UTCI varied within a narrower range, from 32.5 °C to 33.7 °C, at the same grid points (Figure 7b). The larger ranges and spatial standard deviations in the City-LES results indicate that the microscale simulation captured local contrasts in MRT and UTCI within the urban canopy that were smoothed in the WRF fields.

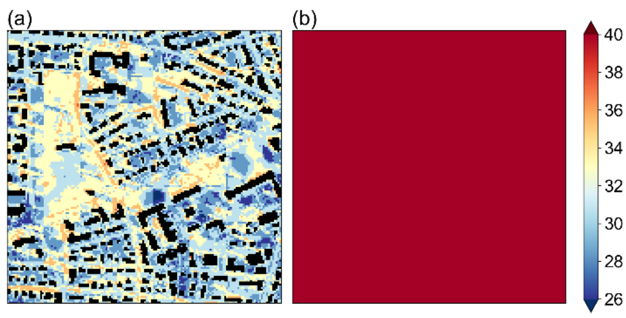

Figure 6. Spatial distribution of mean radiant temperature (MRT) [°C] in the Lozenets district, Sofia, on 16 July 2024: (a) high-resolution City-LES result averaged from 19:50 to 20:00 EEST and (b) MRT derived from the mesoscale WRF output at 20:00 EEST.

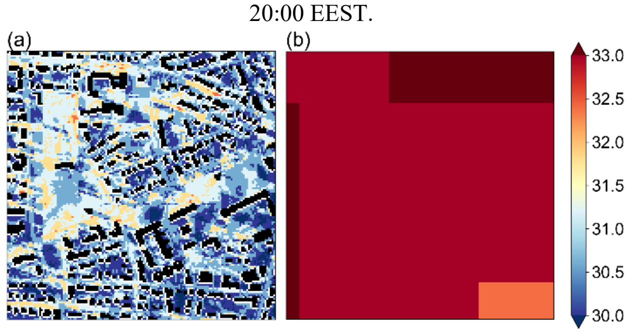

Figure 7. Spatial distribution of the Universal Thermal Climate Index (UTCI) [°C] in the Lozenets district, Sofia, on 16 July 2024: (a) high-resolution City-LES result averaged from 19:50

to 20:00 EEST and (b) UTCI derived from the mesoscale WRF output at 20:00 EEST.

The effect of tree canopies was examined by comparing road cells beneath tree canopies with open road surfaces. Road cells beneath tree canopies had higher MRT and UTCI than open road surfaces, with mean values of 32.9 °C and 31.2 °C, respectively, compared with 31.8 °C and 31.0 °C over open road surfaces. This difference was associated with higher downward longwave radiation beneath tree canopies (462 W m^{-2}) than over open road surfaces (438 W m^{-2}), as well as a smaller net longwave loss at the ground surface (−36.7 W m^{-2} compared with −60.2 W m^{-2}).

The results suggest that the higher MRT and UTCI beneath tree canopies during the analysed period were related to reduced radiative heat loss from the ground to the sky. During 19:50–20:00 EEST, the solar elevation angle was approximately 9°, indicating that direct solar input was already small. Under these late-afternoon conditions, the reduced sky view factor and enhanced downward longwave radiation beneath tree canopies may explain why MRT and UTCI were higher beneath tree canopies than over open road surfaces.

3.3 Effect of Anthropogenic Heat

Figure 8 compares the near-surface air temperature simulated by City-LES with and without AH. The overall spatial pattern of near-surface air temperature was similar between the two simulations (Figure 8a, b). Relatively higher temperatures were found in densely built-up areas, whereas lower temperatures appeared over the park area. The AH-induced temperature difference was generally small, with a domain-averaged value of 0.02 °C, although localized positive differences appeared near building surfaces (Figure 8c).

The median temperature difference was also 0.02 °C, and the 10th–90th percentile range was −0.04 °C to +0.08 °C. In grid cells located within one horizontal grid spacing, or 5 m, of building surfaces, the mean warming was 0.05 °C, suggesting that the AH signal was mainly localized near building surfaces.

The localized AH signal is likely related to the present AH implementation. In the simulation, AH was applied uniformly to building wall and roof surfaces, while road-surface AH was not included. Therefore, the results should be interpreted as a first-order assessment of building-related AH. A more detailed representation of AH sources, including the spatial distribution of building exhaust heat and traffic-related emissions, would be needed to further evaluate AH-induced warming in Sofia.

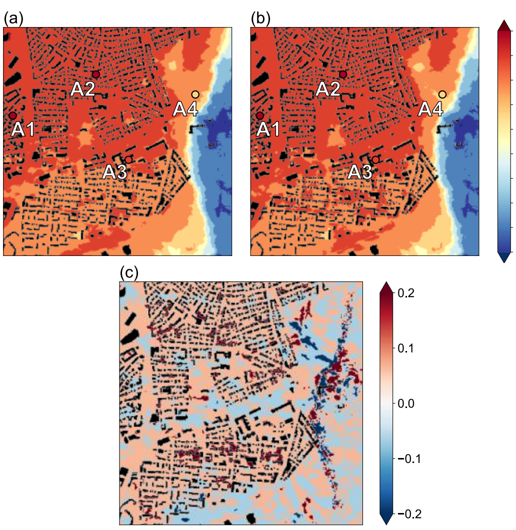

Figure 8. Impact of anthropogenic heat (AH) on near-surface air temperature [°C], simulated by City-LES for 19:50–20:00 EEST on 16 July 2024: (a) without AH, (b) with AH, and (c) difference (with − without AH).

4. Conclusion and Future Work

This study applied a high-resolution WRF–City-LES downscaling approach to simulate the urban thermal environment of the Lozenets district in Sofia, Bulgaria. The conclusions are as follows:

(1) The WRF–City-LES downscaling approach improved the representation of near-surface air temperature at the observation sites. Compared with the mesoscale WRF simulation, the City-LES simulation reduced the MAE from 1.4 °C to 0.3 °C and the RMSE from 1.4 °C to 0.3 °C, while maintaining a high correlation with observations ($r = 0.997$).

(2) City-LES represented finer local temperature variations than WRF within the target district. Near-surface air temperature ranged from 27.7 °C to 34.0 °C in City-LES, compared with 31.2 °C to 33.0 °C in WRF, and the domain-averaged temperature differed among grassland, roads, and building-adjacent areas.

(3) City-LES resolved local variations in outdoor thermal comfort indices. MRT ranged from 25.1 °C to 36.5 °C, whereas UTCI ranged from 29.1 °C to 32.1 °C, indicating city-block-scale differences in thermal comfort related to buildings, tree canopies, and radiative conditions.

(4) The effect of building-related AH on domain-averaged near-surface air temperature was limited under the present implementation. The mean temperature difference was 0.02 °C over the whole domain and 0.05 °C within 5 m of building surfaces, indicating that the AH signal was mainly localized near buildings.

Overall, the WRF–City-LES downscaling framework provides a useful basis for urban climate assessment and future urban digital twin applications, including scenario-based evaluation of heat-mitigation strategies in Sofia.

Although the present study demonstrates the feasibility of the WRF–City-LES downscaling approach for simulating the urban thermal environment in Sofia, several limitations remain. The validation was based on a limited number of observation sites and a single 1 h period on one hot summer day. Future work should apply the framework to multiple cases, introduce time-varying mesoscale boundary conditions, and improve the representation of terrain and AH. Additional observation sites, together with measurements of radiative environments, would also support a more robust validation of spatial variations in thermal comfort indices such as MRT and UTCI.

Acknowledgements

This research was supported by the GATE project, funded by the European Union's Horizon 2020 WIDESPREAD-2018-2020 TEAMING Phase 2 programme under Grant Agreement No. 857155, and by the Programme "Research, Innovation and Digitalisation for Smart Transformation" 2021–2027 (PRIDST) under Grant Agreement No. BG16RFPR002-1.014-0010-C01. We acknowledge access to the Discoverer supercomputer at Sofia Tech Park, Bulgaria.

This work was also supported by the MEXT Promotion of Development of a Joint Usage/Research System Project, Coalition of Universities for Research Excellence Program (CURE), Grant No. JPMXP1323015474, and partly supported by JST SPRING, Grant No. JPMJSP2124. Computational resources of Miyabi were provided through the Multidisciplinary Cooperative Research Program of the Center for Computational Sciences, University of Tsukuba.

References

Agency for Sustainable Energy Development, 2025: Building reports – characteristics. https://portal.seea.government.bg/en/IndustrialSystemsReport (5 June 2026).

Assenova, I. A., Vitanova, L. L., Petrova-Antonova, D., 2024: Urban heat islands from multiple perspectives: Trends across disciplines and interrelationships. *Urban Climate*, 56, 102075. doi.org/10.1016/j.uclim.2024.102075

Bröde, P., Fiala, D., Błażejczyk, K., Holmér, I., Jendritzky, G., Kampmann, B., et al., 2012: Deriving the operational procedure for the Universal Thermal Climate Index (UTCI). *Int. J. Biometeorol.*, 56(3), 481–494. doi.org/10.1007/s00484-011-0454-1

Chen, F., Kusaka, H., Bornstein, R., Ching, J., Grimmond, C. S. B., Grossman-Clarke, S., et al., 2011: The integrated WRF/urban modelling system: development, evaluation, and applications to urban environmental problems. *Int. J. Climatol.*, 31(2), 273-288. doi.org/10.1002/joc.2158

City Living Lab, 2024: Sofia Sensor. GATE Institute. https://citylab.gate-ai.eu/sofiasensors (15 June 2026)

Dudhia, J., 1989: Numerical study of convection observed during the winter monsoon experiment using a mesoscale two-dimensional model. *J. Atmos. Sci.*, 46(20), 3077-3107. doi.org/10.1175/1520-0469(1989)046<3077:NSOCOD>2.0.CO;2

Geoportal of Geodesy, Cartography and Cadastre Agency, 2024: Cadastral and specialized maps [WWW Document]. https://kais.cadastre.bg/en/ (2 October 2025).

Giorgi, F., Mearns, L. O., 1991: Approaches to the simulation of regional climate change: A review. *Rev. Geophys.*, 29(2), 191–216. doi.org/10.1029/90RG02636

Hong, S.-Y., Dudhia, J., Chen, S.-H., 2004: A revised approach to ice microphysical processes for the bulk parameterization of clouds and precipitation. *Mon. Wea. Rev.*, 132(1), 103-120. doi.org/10.1175/1520-0493(2004)132<0103:ARATIM>2.0.CO;2

Ikeda, R., Kusaka, H., Iizuka, S., Boku, T., 2015: Development of urban meteorological LES model for thermal environment at city scale. *9th International Conference on Urban Climate*.

Janjić, Z. I., 1994: The step-mountain eta coordinate model: Further developments of the convection, viscous sublayer, and turbulence closure schemes. *Mon. Wea. Rev.*, 122(5), 927-945. doi.org/10.1175/1520-0493(1994)122<0927:TSMECM>2.0.CO;2

Kain, J. S., 2004: The Kain-Fritsch convective parameterization: An update. *J. Appl. Meteor. Climatol.*, 43(1), 170-181. doi.org/10.1175/1520-0450(2004)043<0170:TKCPAU>2.0.CO;2

Khanh, D. N., Varquez, A. C. G., Kanda, M., 2023: Impact of urbanization on exposure to extreme warming in megacities. *Heliyon*, 9(4), e15511. doi.org/10.1016/j.heliyon.2023.e15511

Koleva, T., Vitanova, L., Petrova-Antonova, D., Kostadinov, A., 2024. Semantic Enrichment and Analysis of Building Energy Consumption Data for the City of Sofia. *IFIP International Conference on Artificial Intelligence Applications and Innovations*. Cham: Springer Nature Switzerland, 462–475. doi.org/10.1007/978-3-031-63227-3_33

Kusaka, H., Ikeda, R., Sato, T., Iizuka, S., Boku, T., 2024: development of a multi-scale meteorological large-eddy simulation model for urban thermal environmental studies: The “City-LES” model version 2.0. *J. Adv. Model. Earth Syst.*, 16(10), e2024MS004367. doi.org/10.1029/2024MS004367

Kusaka, H., Kimura, F., 2004: Coupling a single-layer urban canopy model with a simple atmospheric model: Impact on urban heat island simulation for an idealized case. *J. Meteor. Soc. Japan*, 82(1), 67-80. doi.org/10.2151/jmsj.82.67

Kusaka, H., Kondo, H., Kikegawa, Y., Kimura, F., 2001: A simple single-layer urban canopy model for atmospheric models: Comparison with multi-layer and slab models. *Bound.-Layer Meteorol.*, 101, 329-358. doi.org/10.1023/A:1019207923078

Lee, G. J., Muñoz-Esparza, D., Yi, C., Choe, H. J., 2019: Application of the cell perturbation method to large-eddy simulations of a real urban area. *J. Appl. Meteor. Climatol.*, 58(5), 1125-1139. doi.org/10.1175/JAMC-D-18-0185.1

Liu, J., Gao, H., Jia, R., Wang, R., Han, D., Lin, L., Xu, X., Qiao, Z., 2025: A downscaling framework with WRF-UCM and LES/RANS models for urban microclimate simulation strategy: Validation through both measurement and mechanism model. *Build. Environ.*, 269, 112361. doi.org/10.1016/j.buildenv.2024.112361

Maronga, B., Banzhaf, S., Burmeister, C., Esch, T., Forkel, R., Fröhlich, D., et al., 2020: Overview of the PALM model system 6.0. *Geosci. Model Dev.*, 13(3), 1335. doi.org/10.5194/gmd-13-1335-2020

Muñoz-Esparza, D., Kosović, B., Mirocha, J., van Beeck, J., 2014: Bridging the Transition from mesoscale to microscale turbulence in numerical weather prediction models. *Bound.-Layer Meteorol.*, 153, 409-440. doi.org/10.1007/s10546-014-9956-9

Mlawer, E. J., Taubman, S. J., Brown, P. D., Iacono, M. J., Clough, S. A., 1997: Radiative transfer for inhomogeneous atmospheres: RRTM, a validated correlated-k model for the longwave. *J. Geophys. Res. Atmos.*, 102(D14), 16663-16682. doi.org/10.1029/97JD00237

National Centers for Environmental Prediction, 2000: NCEP FNL Operational Model Global Tropospheric Analyses, continuing from July 1999. NSF National Center for Atmospheric Research. doi.org/10.5065/D6M043C6

Nishi, A., Kusaka, H., Vitanova, L. L., Imai, Y., 2019: Contributions of foehn and urban heat island to the extreme high-temperature event in Niigata City during the night of 23–24 August 2018. *SOLA*, 15, 132–136. doi.org/10.2151/sola.2019-024

Sato, T., Kusaka, H., 2023: Intercomparison of synthetic inflow turbulence generation methods for large-eddy simulation models in thermally driven convective boundary layer simulations. *SOLA*, 19, 165-172. doi.org/10.2151/sola.2023-022

Skamarock, W. C., Klemp, J. B., Dudhia, J., Gill, D. O., Liu, Z., Berner, J., et al., 2019: A description of the Advanced Research WRF model version 4. *NCAR Tech. Note NCAR/TN-556+STR*, 145. doi.org/10.5065/1dfh-6p97

Sofia Municipality, 2009: General Master Plan of Sofia Municipality. https://sofiaplan.bg/Documents/OUP-Sofia_2009_withfonts.pdf Sparrow, E. M., Cess, R. D., 1978: Radiation heat transfer. *Principles of Heat Transfer in Porous Media*, Mechanical Engineering Series, Springer. doi.org/10.1007/978-1-4612-4254-3_5

Thiruridathil, R. P., Dasari, H. P., Alduwais, A. K., Karumuri, R. K., Srinivas, C. V., Hoteit, I., 2024: Performance of PALM-4U/WRF model for simulating the urban meteorology of King Abdullah University of Science and Technology (KAUST), Saudi Arabia. *Urban Climate*, 58, 102162. doi.org/10.1016/j.uclim.2024.102162

TomTom, 2024: TomTom Traffic Stats. https://www.tomtom.com/products/traffic-stats/

Vitanova, L. L., Matsumura, S., Petrova-Antonova, D., 2026: Influence of Muesmann's plan on contemporary urban planning in Sofia City. *City Environ. Interact.*, 29, 100303.

Vitanova, L. L., Petrova-Antonova, D., Shirinyan, E., Khanh, D. N., Trendafilova, T. K., Subasinghe, S., et al., 2026: Fusing urban informatics and weather modelling in digital twins for city-scale heat-health mapping. *Comput. Urban Sci.*, 6, 32. doi.org/10.1007/s43762-026-00268-3

Vitanova, L. L., Petrova-Antonova, D., Hristov, P. O., Shirinyan, E., 2023: Towards energy atlas of Sofia City in Bulgaria. *Int. Arch. Photogramm. Remote Sens. Spatial Inf. Sci.*, XLVIII-1/W2-2023, 123-129. doi.org/10.5194/isprs-archives-XLVIII-1-W2-2023-123-2023

Vitanova, L. L., Kusaka, H., Doan, Q., Subasinghe, S., 2021: How urban growth changes the heat island effect and human thermal sensations over the last 100 years and towards the future in a European city? *Meteorol. Appl.*, 28(4), e2019. doi.org/10.1002/met.2019

Vitanova, L. L., Kusaka, H., 2018: Study on the urban heat island in Sofia City: Numerical simulations with potential natural vegetation and present land use data. *Sustain. Cities Soc.*, 40, 110–125. doi.org/10.1016/j.scs.2018.03.012

Vogel, J., Afshari, A., Chockalingam, G., Stadler, S., 2022: Evaluation of a novel WRF/PALM-4U coupling scheme incorporating a roughness-corrected surface layer representation. *Urban Climate*, 46, 101311. doi.org/10.1016/j.uclim.2022.101311

Washburn, B., 2020: Heron: A QGIS plugin [Source code]. GitHub. https://github.com/blueherongis/Heron (14 July 2026).

Wilby, R. L., Wigley, T. M. L., 1997: Downscaling general circulation model output: A review of methods and limitations. *Prog. Phys. Geogr.*, 21(4), 530–548. doi.org/10.1177/030913339702100403

World Population Review, 2024: Sofia, Bulgaria Population. https://worldpopulationreview.com/cities/bulgaria/sofia (13 March 2026).